STUDY OF GRAPHENE DISPERSIONS IN SODIUM DODECYLSULFATE BY STEADY-STATE FLUORESCENCE OF PYRENE.

S. Vera-López*, P. Martínez, M.P. San Andrés, A. M. Díez-Pascual and M. Valiente

Department of Analytical Chemistry, Physical Chemistry, and Chemical Engineering, University of Alcalá, 28871, Madrid, Spain

*Corresponding author

e-mail: soledad.vera@uah.es

ORCID: 0000-0001-8626-0556

ABSTRACT

Hypothesis

Aqueous solutions of ionic surfactants allow the exfoliation of graphene, that can be explained considering the adsorption model of ionic surfactants to hydrophobic surfaces. For many years, pyrene has been used as a fluorescent probe because its sensitivity to the micro-environment. The study of pyrene fluorescence in the presence of different graphene dispersions in an ionic surfactant, would improve the knowledge of the graphene-surfactant interactions.

Experiments

Different dispersions of graphene in sodium dodecylsulfate were prepared at different weight ratios 0.5, 1 and 2%. The dispersions have been studied by Raman spectroscopy, scanning electron microscopy and transmission electron microscopy. The influence of the dispersions on the pyrene fluorescence has been investigated.

Findings

The graphene sheets modified by the surfactant quench the fluorescence of pyrene, which depends on the amount of graphene, the concentration of surfactant and the weight ratio. For surfactant concentrations below the critical micelle concentration, the quenching effect is higher as the weight ratio increases. Once this concentration is reached, the fluorescence increases slightly and then levels off. This behavior has been explained by the adsorption model. For a constant surfactant concentration, two straight lines can be observed in the Stern-Volmer plots whose cut-off point is approximately 20 mg L^{-1} of graphene.

KEY WORDS: graphene; SDS; pyrene; dispersion; fluorescence quenching

1. Introduction

Graphene (G) is the best known two-dimensional material, consisting of sp^2-hybridized carbon atoms arranged in a honeycomb lattice [1], and its excellent properties make it very attractive for a wide range of applications such as electronics, electromagnetic shielding, barrier coatings, composites, energy storage and sensing, to mention but a few [2-6]. To make a graphene dispersion useful, the nanomaterial should be dispersed in a suitable concentration, in an appropriate solvent, and remain dispersed for a reasonable period of time. However, there are two problems that remain unsolved. The first is the lack of scalable synthetic routes to produce G in the quantities required for industrial applications. The second concerns the poor colloidal stability of graphene in most solvents. Regarding the latter, a colloidal dispersion is a two phases system where one phase (the dispersed phase) is dispersed as very fine particles in the second phase (the continuous phase). In many cases, the system can be quite complex. There may be more than one type of dispersed phase, and any of the phases (dispersed or continuous) may be composed of multiple components, for example, in an aqueous phase there may be electrolytes, surfactants, polymers and other molecular species.

Graphene can be obtained by different methods [4]: a) graphite exfoliation and cleavage, b) chemical vapour deposition of hydrocarbons (CVD), or c) chemically derived graphene, by the conversion of graphite to graphene oxide and subsequent reduction. In recent years, the production of G from graphite has been popularized by sonication assisted liquid-phase exfoliation (LPE) [7] in the presence of organic solvents [8-12], ionic liquids [11,13-15] and aqueous surfactant solutions [7,11,12,16,17]. The last approach offers advantages over the use of solvents which are toxic and expensive. The presence of surfactants, stabilizer molecules of the dispersion, minimizes the free surface energy by non-covalent functionalization, preventing the aggregation of the G sheets.

The use of surfactant aqueous solution for G exfoliation is based on previous works with carbon nanotubes [18,19]. Coleman research group is pioneer in studying the stabilization of G in surfactant solutions and the characterization of the resulting materials [20-22]. Lotya *et al*. [20] used sodium dodecylbenzenesulfonate (SDBS) to obtain G from graphite exfoliation. According to transmission electron microscopy (TEM) images, the dispersed phase was composed of small graphitic flakes: 40% of them comprised less than five layers and about 3% were monolayers. The same research group dispersed G in water via stabilization with 12 ionic and non-ionic surfactants [21]. The concentration of G dispersed was found to be dependent on the type of surfactant. Thus, for ionic surfactants the concentration increased with the square of the zeta potential of the surfactant coated flakes, hence it is proportional to the magnitude of the electrostatic potential barrier that stabilizes the surfactant coated flakes against aggregation, while for non-ionic surfactants the concentration rose linearly with the magnitude of the steric potential barrier stabilizing the flakes.

An important question concerning the use of surfactants as G dispersants is related to their concentration: below or above the critical micelle concentration, CMC?. According to preceding studies [10-12,23-25], solutions of surfactants both above and below the CMC can be used for G dispersion. It is reasonable to believe that at concentrations above the CMC there is a competitive phenomenon between micelle formation and surfactant adsorption on the G surface, thereby destabilizing the dispersion.

Over the past years, pyrene has been widely used as fluorescent probe for micro-heterogeneous systems such as micelles [26-30]. The fluorescence emission spectrum of pyrene is characterized by an ensemble of five major vibronic bands, designated as I, II, III, IV and V, with well-defined peaks at ~374, 379, 384, 394 and 410 nm, respectively. They are attributed to $\pi \rightarrow \pi^*$ transitions and are cumulatively referred to as the monomeric emission. The peak at 374 nm corresponds to the first vibronic band, while that at 384 nm is attributed to the third vibronic

band. Since the electronic and vibronic states are coupled, band III is exquisitely sensitive to the polarity of the probe's microenvironment. It shows increased fluorescence emission intensity in comparison to that of band I in hydrophobic environments, while lower intensity in polar environments [27,31,32]. The ratio of the fluorescence intensities of the first and third vibronic bands of pyrene (I/III) generally increases upon increasing the polarity of the microenvironment.

The current work is devoted to study different G dispersions in sodium dodecylsulfate (SDS) by steady-state fluorescence using pyrene as a probe. It has three main objectives: a) to evaluate the quality of the dispersions, i.e. level of G exfoliation, by SEM, TEM and Raman analysis, and statistical comparison of the obtained dispersions by measuring the fluorescence of pyrene, b) to compare the polarity microenvironment of aqueous SDS solutions and G dispersions in SDS by determining the ratio of the fluorescence intensities of the first and third vibronic bands of pyrene, and c) to study the quenching of the fluorescence of pyrene.

2. Experimental

2.1 Chemicals

Pyrene and SDS were purchased from Sigma-Aldrich. Pristine graphene (avan-GRAPHENE) with lamellar structural morphology comprising 1-2 layers with a thickness ≤ 2 nm was provided in powder form by Avanzare Innovación Tecnológica, SL (Logroño, Spain). A detailed characterization of the raw nanomaterial is given in Figures S1 and S2 (Supplementary Material).The stock solution of pyrene was prepared by dissolving the appropriate amount in methanol (HPLC grade from Scharlab, Madrid, Spain). The SDS aqueous solution was prepared using ultrapure water (Milli-Q system, Milford, USA).

2.2 Instrumentation.

Fluorescence spectra of pyrene in aqueous SDS solutions and in the dispersions of graphene in SDS were recorded at 25±1 °C with a PerkinElmer LS-50B luminescence

spectrometer equipped with a Xe flash lamp and quartz cuvettes of 1 cm path length thermostatised with a Thermomix BU bath. The excitation and emission slit widths were 5 nm and the scan speed 600 nm min^{-1}. Data acquisition was carried out using the Perkin-Elmer Flwin Lab software. An ultrasonic bath from Selecta and a Hielscher UP400S ultrasonic homogenizer were used for the preparation of the dispersions; centrifugation was carried out using an Orto Alresa Digicen centrifuge. The morphology of the samples was studied by scanning electron microscopy (SEM), using a Zeiss DSM-950 microscope (Carl Zeiss, Germany), operating at 15 kV and different magnifications. The G dispersions in the surfactant were allowed to dry for several days and were coated with a 50 nm gold layer to facilitate observation and avoid accumulation of charges during irradiation with the electrons. The dispersions were also observed by transmission electron microscopy (TEM) using a Zeiss EM-10C/CR instrument. Samples for TEM measurements were prepared by depositing a drop of the liquid graphene dispersion onto 400 mesh copper grids coated with formvar carbon film (Aname SL, Madrid, Spain). Then, the samples were dried at room temperature overnight. Raman measurements were performed with a Thermo Scientific DXR Raman Microscope with a solid-state laser at an excitation wavelength of 532 nm. Elemental analysis of raw G was carried out with a LECO CHNS-932 elemental analyzer.

2.3 Preparation of graphene dispersions in SDS.

G dispersions were prepared via surfactant-assisted sonication. In short, the appropriate amount of G was weighted and added to a 0.02 mol L^{-1} aqueous SDS solution to have weight ratios G/SDS (w_G/w_S) of 0.5, 1.0 and 2.0%. Subsequently, the solutions were held for 1 hour in the ultrasonic bath and then sonicated with the ultrasonic device for 10 minutes at a power of 160 W. Finally, the dispersions were centrifuged for 1 hour at 4000 rpm; the supernatant was stored for fluorescence and TEM measurements while the solid residue was used for Raman and SEM evaluation.

Two different series of diluted dispersions were prepared: one by varying the concentration of G and the surfactant simultaneously via dilution with water while maintaining the w_G/w_S weight ratio constant and equal to 0.5, 1 and 2%, and the other by keeping the SDS concentration fixed at 0.02 mol L^{-1} and changing the amount of G via dilution with the surfactant solution in order to obtain different w_G/w_S weight ratios. All the dispersions were prepared in duplicate to ensure for repeatability.

2.4 Fluorescence of pyrene.

The fluorescence of pyrene (15 μg L^{-1}) was measured in aqueous SDS solutions both below and above the CMC as well as in the two-different series of G/SDS dispersions mentioned above. All fluorescence spectra were performed in triplicate and normalized with the band at 374 nm.

To confirm the excitation and emission wavelength data for SDS solutions and G dispersions in SDS, the three-dimensional excitation-emission matrix (3DEEM) spectra were recorded by scanning over an excitation wavelength between 300 and 400 nm at an increment of 5 nm, and an emission wavelength in the range of 350-450 nm. The 3DEEM spectra are shown as elliptical contours where the abscissa represents the emission wavelength while the ordinate shows the excitation wavelength and the contour line indicates the fluorescence intensity.

2.5 Statistical methods.

All statistical calculations were performed using Statgraphics Centurion software.

3. Results and discussion

3.1 Characterization of graphene dispersions in SDS.

The quality of G dispersions in 0.02 mol L^{-1} aqueous SDS solutions was assessed by SEM, TEM and Raman spectroscopy. SEM and TEM analysis were carried out to get an insight into the overall level of dispersion and exfoliation of G nanosheets. Raman spectroscopy is a

valuable tool to obtain information about the concentration of defects in graphene sheets and their level of exfoliation [33,34].

The results of an elemental analysis performed on pristine G are: 91.08 %C, 1.83%H, 1.38%N and 5.71%O.The oxygen content agrees well with that determined by the manufacturer via XPS (5.2%). The X-ray diffraction pattern (XRD) of pristine G is shown in Figure S1 (Supplementary Material). G exhibits a characteristic sharp peak at $2\theta = 25.87^{o}$ related to the (002) reflection of graphite which corresponds to a d spacing of 0.344 nm, and a small peak at $2\theta = 44.0^{o}$ related to the (101) reflection. However, the (002) reflection of pure graphite appears at 26.50^{o} [35], corresponding to a d-spacing of 0.336 nm. This small increase in the d-spacing is ascribed to the presence of some oxygen-containing groups located at the sheet edges and above the sheets surface.

Figure S2 shows the IR spectrum of G. The peak at ~3400 cm-1 corresponds to O–H stretching vibrations and that at about 1720 cm^{-1} is characteristic of the C=O stretching of carboxylic acid groups. The band at ~1400 cm^{-1} corresponds to the O–H deformation and those at 1230 and 1050 cm^{-1} are related to epoxy C–O stretching vibrations [36]. These features confirm the presence of a few oxygen-bearing functional groups, as indicated by XPS analysis, mainly epoxy, carboxyl acid and hydroxyl, that are likely covalently bonded to sp3 carbon atoms located at defect sites of the basal plane and at the edges. Hence, it can be concluded that the raw nanomaterial more closely resembles reduced graphene oxide (rGO) than hydrophobic pristine graphene.

The Raman spectra of pristine graphene and the corresponding G dispersions in SDS (w_G/w_S 0.5, 1 and 2%) are compared in Fig. 1. The four peaks in the Raman spectrum of graphene are the disorder-induced D band at 1345 cm^{-1} attributed to structural disorder at defect sites [37], the tangential G band at 1583 cm^{-1} that arises from in-plane vibrations of sp^2 bonded carbon atoms in graphene sheets, the G'-band at 2672 cm^{-1}, a second-order overtone of the D-band which

shape, position and width depends on the number of graphene layers [38] and the D+G band at 2930 cm^{-1} that results from the combination of the two modes that give rise to the first-order D and G bands and it is caused by lattice disorder.

The spectra of the dispersions in SDS are qualitatively similar to that of raw graphene, and show the four aforementioned bands, albeit these exhibit different intensity and peak positions. A gradual decrease in the intensity of both D and G bands is found with increasing w_G/w_S weight ratio. The D to G band intensity ratio (I_D/I_G) provides quantitative information about the number of defects in a graphene sheet: the lower the ratio, the lower the disorder. The calculated I_D/I_G values for pristine graphene and the 0.5, 1 and 2 % dispersions in SDS are 1.17, 1.15, 1.15 and 1.13, respectively. Since there is hardly change in the I_D/I_G ratio upon graphene dispersion in the surfactant, it can be concluded that the structural order of the sheets is maintained after the ultrasonication process used in this work, that is, the integrity of the graphene network is preserved, which is essential to maintain its properties. This contrasts with the results reported for graphene dispersed in high concentrations of the anionic surfactant sodium cholate [22], where the I_D/I_G ratio increased after the sonication step, and corroborate the strong influence of the sonication parameters, namely power and time, on the type and quality of the dispersions obtained.

On the other hand, a small shift of the G band towards higher wavenumber is found in the presence of SDS, hinting towards surfactant-graphene interactions. Accordingly, the change in the position of the G band is attributed to the alteration of the electronic structure of graphene [39]: the band appears at higher frequency in the presence of electron-acceptor molecules. The sulfate groups of SDS make it an electron-acceptor molecule, hence causing a blue shift of the G band. It is also important to analyze the change in the position and intensity of the 2D band after dispersion in the surfactant. As can be observed, a gradual shift towards higher wavenumbers occurs upon increasing w_G/w_S mass ratio, from 2672 cm^{-1} for pristine graphene to 2706 cm^{-1} for

the 2 % dispersion. This upshift is indicative of graphene delamination into thinner layers [22], corroborating that the ultrasonication process induced graphene exfoliation. Further, the 2D band has higher intensity in single layer than in multi-layer graphene [40], yet another confirmation of the successful exfoliation of the nanomaterial in the presence of SDS.

Another evidence of the gradual exfoliation upon increasing w_G/w_S weight ratio can be obtained from the position of the D+G band, which steadily shifts to higher wavenumber, phenomenon that has also be related to a decrease in the number of graphene layers [41]. All the aforementioned features found in the Raman spectra are consistent with SEM observations, Fig. 2, the sheets are wrinkled and bended, showing a high degree of flexibility. In addition, TEM images, Fig.3, reveal very thin well-defined G sheets for the dispersions. The sheets are disentangled and disaggregated, albeit the lack of individual monolayers corroborates that G is not fully exfoliated. Further, many number of black spots can be observed within the sheets or in their surface, attributed to self-arranged and/or aggregated SDS molecules, since these dispersions have a high amount of surfactant.

3.2 Fluorescence of pyrene in SDS aqueous solutions and graphene dispersions in SDS.

Fig. S3a and S3b (Supplementary Material) show, as an example, the 3DEEM spectra of pyrene (15 μg L^{-1}) in 0.02 mol L^{-1} SDS aqueous solution and in G (w_G/w_S = 0.5%) dispersion, respectively. The typical values of excitation wavelength of pyrene (320 and 335 nm) can be observed, indicating that they are not affected by the presence of the G dispersion. Further, three of the emission bands of pyrene, I (374 nm), III (384 nm) and V (394 nm) are detected, corroborating that the emission wavelengths are not altered either in the G dispersion. From this point onwards, all the fluorescence measurements have been carried out with an excitation wavelength of 335 nm that leads to the emission spectra with the maximum sensitivity.

Firstly, the effect of SDS concentration, both below and above the CMC, on the fluorescence of pyrene was investigated. Fig.4 shows the normalized fluorescence spectra of pyrene in aqueous solutions of different SDS concentrations. At concentrations below the CMC, the emission bands I and V can be observed, showing intensity values similar to those found in the absence of surfactant. Upon increasing the SDS concentration above the CMC, the band III begins to be defined. This behavior is indicative of the presence of micelles in the medium, and pyrene is located in the micellar phase [27,31,32]. At concentrations below the CMC there is some variability in the fluorescence data. However, once the CMC is exceeded, the fluorescence intensity remains constant and is higher than that found in the absence of SDS, thus confirming the interaction of the pyrene with the micelles.

The change in the fluorescence of pyrene a) with the concentration of both G and SDS, at a constant w_G/w_S, and b) with the concentration of G, at a constant SDS concentration of 0.02 mol L^{-1}, was studied. Fig.5a and 5b show the emission spectra for w_G/w_S ratio constant, 0.5 and 2% respectively, for SDS concentrations both below and above the CMC. Similar behavior was observed for w_G/w_S = 1%. In all cases, the fluorescence intensity decreases with increasing SDS concentration below the CMC, an effect that is more pronounced for w_G/w_S = 2%. Above the obtained for dispersions with different G concentration at a fixed SDS concentration of 0.02 mol L^{-1} (Fig.5c and 5d) reveal a continuous decrease in intensity upon raising G content, corroborating that the higher the G content, the stronger the quenching effect is.

Fig.6 describes this behavior more clearly. Fig. 6a shows the evolution of the fluorescence of pyrene as a function of the SDS concentration, at a constant w_G/w_S ratio. For comparative purposes, the effect of a surfactant solution without G on the fluorescence intensity has also been included in the plot. Clearly, the quenching effect is stronger for G dispersions compared to the SDS aqueous solution. For SDS concentrations below the CMC, the quenching effect becomes more pronounced as the w_G/w_S ratio increases. Once the CMC is reached, the fluorescence

increases slightly and then levels off. Fluorescence data show a discontinuity at a concentration that corresponds to the CMC, similar to the trend found by other authors [30,42], with a value of $8.3x10^{-3}$ mol L^{-1} which was in close agreement with the values reported in the literature [43]. This fact assumes that the presence of G does not modify the formation of SDS micelles in the bulk solvent. The variation of the pyrene fluorescence with the G concentration, for the dispersions at a fixed SDS concentration of 0.02 mol L^{-1} is plotted in Fig.6b. It is pointed out that SDS concentration is constant and higher than the CMC, so that micelles are present in these G dispersions and the decrease in fluorescence values follows a very different trend to that observed in Fig.6a. A continuous quenching process with concentration of G was observed.

The behaviour observed can be explained considering the adsorption model of ionic surfactants on hydrophobic surfaces. G flakes are first exfoliated by sonication-induced cavitation and shear force, and subsequently they adhere to the charged surfactant molecules. The adsorption of ionic surfactants on hydrophobic surfaces such as G does not fit to the Langmuir adsorption isotherm model. SDS adsorption on graphitized carbon black, known as Graphon, shows two separate steps. The first stage is the formation of a close-packed monolayer with molecules located horizontally on the hydrophobic surface. The second step, near the CMC, corresponds to a monolayer oriented perpendicular to the surface with the head groups away from the solid [44]. This approach was also described by Hsieh et al. [45] to explain the stability of dispersions of functionalized graphene in SDS at different concentrations of surfactant. The authors proposed four steps: a) adsorption of isolated surfactant monomers, b) adsorption of a surfactant monolayer, c) formation of hemi-cylindrical surface micelles, and d) formation of micelles in bulk solution. The concentration of surfactant required for the formation and adsorption of the hemi-micelles is defined as critical surface aggregation concentration, CSAC.

For organic molecules like pyrene, it has been demonstrated that in addition to the hydrophobic effect, π-π interactions are responsible for the strong affinity toward the basal plane

of G and its derivatives [46-49]. The adsorption of organic molecules is a noncovalent functionalization of G involving π-π stacking interactions, and according to Wang et al. [50], the FTIR spectra of G upon adsorption of polycyclic aromatic hydrocarbons corroborate that π-π stacking interactions play an important role in the molecular process. These interactions cause the quenching of fluorescence observed for the pyrene molecule at surfactant concentrations below the CSAC, when the hemi-micelles are not adsorbed to the G surface.

Bearing all this in mind, the different steps of surfactant adsorption at the G surface, as well as the explanation for the observed effect on the pyrene fluorescence can be proposed, Fig. 7. Four steps can be distinguished, depending on the concentration of SDS: **1** close-packed monolayer with molecules located horizontally on the hydrophobic surface, **2** monolayer oriented perpendicular to the surface, **3** formation and adsorption of hemi-micelles at the CSAC, and **4** micelles formation in the bulk solution at the CMC. Regarding the pyrene location, it is likely adsorbed onto G in steps **1** and **2**. Above the CSAC, pyrene is solubilised into the hemi-micelles, step **3**. Above the CMC, a partition equilibrium of pyrene between the micelles in the bulk solution and the hemi-micelles onto the G surface is established, step **4**.

As can be observed in Fig.6a, fluorescence data at [SDS] < CMC can be fitted to two straight lines with different slopes; the lines are well defined for w_G/w_S = 1 and 2%, whilst are more ambiguous for w_G/w_S = 0.5%. This situation would correspond to the transition from step **1**-**2**, indistinguishable from each other, to step **3,** new formation and adsorption of hemi-micelles, and the CSAC values can be determined as the cut-off point of the straight lines. Thus, a CSAC value of about $2x10^{-3}$ mol L^{-1} has been calculated using the data for G weight ratios of 1 and 2%. However, due to the variability of the data for the dispersion with 0.5% G, it was not possible to obtain an accurate value of the CSAC.

Systematically, the most prominent decay in the fluorescence intensity is found for G dispersions without any surfactant aggregates. In steps **1** and **2**, without surfactant aggregates in

the medium, pyrene tends to interact with a slightly modified G due to the adsorption of monomers, and the drop-in fluorescence intensity is very pronounced (high slope). When step **3** is reached, the reduction in intensity becomes less pronounced, until the CSAC value is exceeded. The pyrene molecule is located in a friendly environment formed by the hemi-micelles and somewhat detached from the G surface. Above the CMC, there is a partition equilibrium of pyrene between the micelles and G modified with hemi-micelles. Therefore, it can be concluded that the partition coefficient is much lower than 1, which means that the amount of pyrene in the micellar phase is considerably smaller than that within G modified by the hemi-micelles. When the SDS concentration remains constant and above the CMC, Fig.6b, this situation appears to be the only one possible, hence the fluorescence decreases with increasing G concentration.

To complete the study of the fluorescence of pyrene in the presence of G/SDS dispersions, the ratio of the fluorescence intensities of the first and third vibronic bands (I/III) was calculated for w_G/w_S = 0.5, 1 and 2%. Fig.8 shows the change in the I/III intensity ratio with SDS concentration; data for SDS aqueous solutions without G were also included for comparison. Systematically, the data follow the typical trend of a sigmoidal curve [26-30]. For SDS concentrations below the CMC, the I/III ratio ranges from 1.4 to 1.6, which corresponds to a polar microenvironment. The I/III ratio decreases and reaches a value of ≈1.0, indicative of a hydrophobic microenvironment, at concentrations higher than the CMC. It is interesting to note that, according to the I/III values, at [SDS]> CMC, the environment of the G/SDS dispersions is very similar to that obtained for SDS micelles. This indicates that the polarity experienced by pyrene hardly changes upon addition of graphene, since likely pyrene is still solvated by methanol as suggested by de Miguel et al [51]. Therefore, graphene superficially modified by adsorption of hemi-micelles is a suitable environment for pyrene in terms of hydrophobicity, and, as mention,ned previously, pyrene does not tend to localize inside the micelles in the bulk solution.

3.3 Statistical comparison of graphene dispersions in SDS by fluorescence data of pyrene.

As indicated in the Experimental section, G (0.5, 1 and 2%) dispersions in SDS 0.02 mol L^{-1} were prepared in duplicate, (Set 1 and Set 2), and the fluorescence spectra of pyrene were measured in triplicate. To assess the presence of statistically significant differences, P = 0.05, between both sets of dispersions for each w_G/w_S ratio, the average fluorescence intensity values of bands I, III and V (374 nm, 384 nm and 394 nm) of pyrene obtained for Set 1 (X axis) were plotted versus the average values of Set 2 (Y axis). If there are no statistically significant differences for the given confidence value, a straight line with intercept 0 and slope 1, null hypothesis H_0, should be obtained [52].

According to Table S1 (Supplementary Material), for G/SDS dispersions with w_G/w_S constant, except for w_G/w_S = 1%, the null hypothesis formulated for the intercept should be rejected, P <0.05. This means that the two sets of dispersions with w_G/w_S = 0.5 and 2% show statistically significant differences, for the proposed confidence level. The results for w_G/w_S = 2% are surprising, since the data show good homogeneity (Fig.6a). Regarding the dispersions with variable w_G/w_S at a fixed SDS concentration (Table S2 in Supplementary Material), no statistically significant differences are found between the two sets of dispersions for the three w_G/w_S investigated. Therefore, the null hypothesis is accepted for the intercept and slope values, P> 0.05. On the whole, despite the difficulties inherent to the preparation of G dispersions in aqueous surfactant solutions, no systematic errors are in general present.

3.4 Quenching of pyrene fluorescence by graphene dispersions in SDS.

The term “fluorescence quenching” is applied to any process that decreases the fluorescence intensity of a fluorophobe. A great variety of interactions can produce the quenching phenomenon: reactions in the excited state, molecular rearrangement, energy transfer, formation

of complexes in the ground state (static quenching), and collisions (dynamic quenching). Collisional or dynamic quenching of fluorescence is described by the Stern-Volmer equation, $F_0/F = 1 + K_{SV}[Q]$, where F_0 and F are the fluorescence intensity in the absence and in the presence of quencher, respectively, [Q] indicates the quencher concentration, and Ksv is the Stern-Volmer constant. For a static quenching, by means of the association constant for complex formation (Ks), it is possible to obtain the variation of the fluorescence intensity with the quencher concentration: $F_0/F = 1 + K_S[Q]$. The resulting equation is similar to the Stern-Volmer relationship [53].

The quenching of pyrene fluorescence was initially studied using the values of band I (374 nm). Fig.S4, see Suplementary Material, shows F_0/F *vs* G concentration for the dispersions with w_G/w_S constant. The fit to the Stern-Volmer equation was only carried out for [SDS] < CSAC, concentration range that corresponds to the most pronounced quenching according to Fig.6a. As can be observed in Fig.S4, the data follow a linear trend up to a G concentration close to 9 mg L^{-1}. The slope of the dispersion with w_G/w_S = 0.5% is significantly smaller than those of the dispersions with w_G/w_S = 1 and 2%, which are very close. Therefore, it is not possible to obtain the values of the quenching constant due to the errors in the linear fit.

Fig.9 shows F_0/F vs G concentration for the dispersions with variable w_G/w_S at a fixed SDS concentration. Two linear regions are observed, which can be associated with two quenching processes dependent on the G concentration. This behaviour has been previously reported for the quenching of the fluorescence of different organic dyes by carbon nanotubes [54], graphene [51,55-57] and graphene oxide [58]. Interestingly, for the three w_G/w_S studied, the data can be fitted to two straight lines whose cut-off point is approximately 20 mg L^{-1}. Therefore, data fit well to the Stern-Volmer equation until a G concentration of 20 mg L^{-1} (inset in Fig.9), and according to Table I, which collects the parameters obtained from the regression analysis, almost 98% of the variability of the data is explained. In this case, the intercept values do not differ

significantly from 1, P = 0.05, and the slope values (quenching constants) are very similar regardless of the G weight percentage.

An analysis of the variance (ANOVA) test at 95% confidence level, P = 0.05, was used to determine whether the differences between the mean values of the slopes obtained from the fit to the Stern-Volmer equation for the two sets of dispersions (Set 1 and Set 2) were statistically significant. The mean values of the slopes along with their standard deviation and relative standard deviation (RSD) are collected in Table IIa. The test was applied to the three G dispersions (w_G/w_S = 0.5, 1 and 2%) in SDS 0.02 mol L^{-1} and the three pyrene bands: 374 nm, 384 nm and 394 nm.

A one-way ANOVA test was applied to the aforementioned data, and the results are gathered in Table IIb. A $P_{value} > 0.05$ (0.978) was obtained, which corroborates that the slope values are not statistically different. Hence, the quenching constant is $0.042 \pm 2x10^{-3}$ L mg^{-1} irrespective of the w_G/w_S weight ratio.

4. Conclusions

Based on the hypotheses formulated, this work focuses on the adsorption of surfactants onto G, and the equilibrium distribution of an aromatic compound between the surfactant aggregates and G. A major challenge when preparing G dispersions is their low reproducibility; therefore, for the first time, a statistical study has been carried out to assess the quality of the dispersions in terms of reproducibility. The difficulty of preparing G dispersions in a surfactant, SDS, is demonstrated when its concentration is below the CMC. However, no statistically significant differences are found when the [SDS]> CMC. More efforts are needed to solve the problem on the preparation of dispersions with carbon nanomaterials in order to obtain more reliable results. The level of G exfoliation depends on the G/SDS weight ratio, w_G/w_S, as revealed by Raman spectroscopy, SEM and TEM [22,40,41]. A quenching of pyrene fluorescence has

been found in the presence of G/SDS dispersions, which can be associated with π-π interactions between aromatic molecules and G [46-50]. A large number of articles dealing with the fluorescence quenching of aromatic compounds by G dispersions in surfactants have been reported. However, the role of different surfactant aggregates and their interactions with graphene and aromatic molecules has not been studied yet. In this work, the fluorescence quenching has been explained in terms of the different surfactant aggregates that are formed and their interaction with both the G surface and the pyrene molecule. At concentrations of SDS below the CMC, where only monomers exist, a very marked fluorescence quenching is observed until the critical surface aggregation concentration, CSAC, due to π-π interactions. At higher concentrations, the quenching is weaker, and it is caused by the presence of monomers and hemi-micelles adsorbed on G [45]; pyrene is located in an environment formed by the hemi-micelles and somewhat detached from the G surface. Above the CMC, the fluorescence values tend to increase, indicating a competitive distribution of pyrene between the modified G and the micelles in the bulk solvent, although the distribution coefficient is lower than 1. The ratio of the fluorescence intensity of bands I/III of pyrene [26-30] reveals that the presence of G does not modify the CMC value of SDS neither the hydrophobicity of the microenvironment of pyrene molecules. The fluorescence quenching obtained for G dispersions at a constant SDS concentration of 0.02 mol L^{-1} has been fitted to a Stern-Volmer equation, and the same quenching constant has been obtained for the three G/SDS weight ratios used in this work (w_G/w_S = 0.5, 1 and 2%). According to the results obtained herein, it will be interesting to compare the behavior of the fluorescence probe when another type of aggregates, such as cylindrical micelles and phases of lyotropic liquid crystals, are present in the G dispersion.

Acknowledgements

The authors gratefully acknowledge the valuable help of Dr. Carmen García Ruíz and Dr. María López López for performing the Raman spectra measurements. We also wish to thank Avanzare Innovacion Tecnologica SL for providing characterization data of the raw nanomaterial. Financial support from the University of Alcalá (Project CCG2015/EXP005) and from the Ministerio de Economía y Competitividad (MINECO, Government of Spain) (Project CTQ2015-66575-P) are gratefully acknowledged. Dr. A.M. Díez-Pascual wishes to acknowledge the MINECO for a "Ramón y Cajal" Postdoctoral Fellowship (RYC-2012-11110) co-financed by the European Union.

References

[1] K.S. Novoselov, A.K. Geim, S.V. Morozov, D. Jiang, Y. Zhang, S.V. Dubonos, I.V. Grigorieva, A.A. Firsov, Electric field effect in atomically thin carbon films, Science 306 (2004) 666-669.

[2] Y. Zhu, S. Murali, W. Cai, X. Li, J.W. Suk, J.R. Potts, R.S. Ruoff, Graphene and graphene oxide: synthesis, properties, and applications, Adv. Mater. 22 (2010) 3906-3924.

[3] X. Cui, C. Zhang, R. Hao, Y. Hou, Liquid-phase exfoliation, functionalization and applications of graphene, Nanoscale 3 (2011) 2118–2126.

[4] V. Singh, D. Joung, L. Zhai, S. Das, S.I. Khondaker, S. Seal, Graphene based materials: past, present and future, Prog. Mater. Sci. 56 (2011) 1178-1271.

[5] F. Perreault, A. Fonseca de Faria, M. Elimelech, Environmental applications of graphene-based nanomaterials, Chem. Soc. Rev. 44 (2015) 5861-5896.

[6] X. Yu, W. Zhang, P. Zhang, Z. Su, Fabrication technologies and sensing applications of graphene-based composite films: advances and challenges, Biosens. Bioelectron. 89 (2017) 72-84.

[7] A. Ciesielski, P. Samorì, Graphene via sonication assisted liquid-phase exfoliation, Chem. Soc. Rev. 43 (2014) 381-398.

[8] Y. Hernandez, V. Nicolosi, M. Lotya, F.M. Blighe, Z. Sun, S. De, I.T. McGovern, B. Holland, M. Byrne, Y.K. Gunko, J.J. Boland, P. Niraj, G. Duesberg, S. Krishnamurthy, R. Goodhue, J. Hutchison, V. Scardaci, A.C. Ferrari, J.N. Coleman, High-yield production of graphene by liquid-phase exfoliation of graphite, Nat. Nanotechnol. 3 (2008) 563-568.

[9] J.N. Coleman, Liquid phase exfoliation of nanotubes and graphene, Adv. Funct. Mater. 19 (2009) 3680-3695.

[10] J.N. Coleman, Liquid exfoliation of defect-free graphene, Acc. Chem. Res. 46 (2013) 14-22.

[11] Y. Wei, Z. Sun, Liquid-phase exfoliation of graphite for mass production of pristine few-layer graphene, Curr. Opin. Colloid Interface Sci. 20 (2015) 311-321.

[12] D.W. Johnson, B.P. Dobson, K.S. Coleman, A manufacturing perspective on graphene dispersions, Curr. Opin. Colloid Interface Sci. 20 (2015) 367-382.

[13] X. Wang, P.F. Fulvio, G.A. Baker, G.M. Veith, R.R. Unocic, S.M. Mahurin, M. Chi, S. Dai, Direct exfoliation of natural graphite into micrometre size few layers graphene sheets using ionic liquids, Chem. Commun. 46 (2010) 4487-4489.

[14] D. Nuvoli, L. Valentini, V. Alzari, S. Scognamillo, S.B. Bon, M. Piccinini, J. Illescas, A. Mariani, High concentration few-layer graphene sheets obtained by liquid phase exfoliation of graphite in ionic liquid, J. Mater. Chem. 21 (2011) 3428-3431.

[15] S. Ravula, S.N. Baker, G. Kamath, G.A. Baker, Ionic liquid-assisted exfoliation and dispersion: stripping graphene and its two-dimensional layered inorganic counterparts of their inhibitions, Nanoscale 7 (2015) 4338-4353.

[16] J. Texter, Graphene dispersions, Curr. Opin. Colloid Interface Sci. 19 (2014) 163-174.

[17] R. Narayan, S.O. Kim, Surfactant mediated liquid phase exfoliation of graphene, Nano Convergence 2:20 (2015) http://link.springer.com/article/10.1186/s40580-015-0050-x?view=classic (accessed Nov 27, 2016)

[18] L. Vaisman, H.D. Wagner, G. Marom, The role of surfactants in dispersion of carbon nanotubes, Adv. Colloid Interface Sci. 128 (2006) 37-46.

[19] R. Rastogi, R. Kaushal, S.K. Tripathi, A.L. Sharma, I. Kaur, L.M. Bharadwaj, Comparative study of carbon nanotube dispersion using surfactants, J. Colloid Interface Sci. 328 (2008) 421-428.

[20] M. Lotya, Y. Hernandez, P.J. King, R.J. Smith, V. Nicolosi, L.S. Karlsson, F.M. Blighe, S. De, Z. Wang, I.T. McGovern, G.S. Duesberg, J.N. Coleman, Liquid phase production of graphene by exfoliation of graphite in surfactant water solutions, J. Am. Chem. Soc. 131 (2009) 3611-3620.

[21] R.J. Smith, M. Lotya, J.N. Coleman, The importance of repulsive potential barriers for the dispersion of graphene using surfactants, New J. Phys. 12 (2010) 125008-125019.

[22] M. Lotya, P.J. King, U. Khan, S. De, J.N. Coleman, High-concentration, surfactant-stabilized graphene dispersions, ACS Nano 4 (2010) 3155-3162.

[23] S.M. Notley, Highly concentrated aqueous suspensions of graphene through ultrasonic exfoliation with continuous surfactant addition, Langmuir 28 (2012) 14110-14113.

[24] W. Du, X. Jiang, L. Zhu, From graphite to graphene: direct liquid-phase exfoliation of graphite to produce single- and few layered pristine graphene, J. Mater. Chem. A 1 (2013) 10592-10606.

[25] S. Wang, M. Yi, Z. Shen, The effect of surfactants and their concentration on the liquid exfoliation of graphene, RSC Adv. 6 (2016) 56705-56710.

[26] K. Kalyanasundaram, J.K. Thomas, Environmental effects on vibronic band intensities in pyrene monomer fluorescence and their application in studies of micellar systems, J. Am. Chem. Soc. 99 (1977) 2039-2044.

[27] M. Almgren, F. Grieser, J.K. Thomas, Dynamic and static aspects of solubilization of neutral arenes in ionic micellar solutions, J. Am. Chem. Soc. 101 (1979) 279-291.

[28] N.J. Turro, P-L Kuo, Fluorescence probes for aqueous solutions of nonionic micelles, Langmuir 1 (1985) 170-172.

[29] J.H. Mathias, Fluorescence study of premicellar aggregation in cationic gemini surfactants, Langmuir 17 (2001) 6148-6154.

[30] L. Piñeiro, M. Novo, W. Al-Soufi, Fluorescence emission of pyrene in surfactant solutions, Adv. Colloid Interface Sci. 215 (2015) 1-12.

[31] A. Nakajima, Intensity enhancement induced by solute-solvent interaction between pyrene and polar solvents, Spectrochim. Acta A Mol. Biomol. Spectrosc. 38 (1982) 693-695.

[32] P. Bandyopadhyay, A.K. Ghosh, S. Bandyopadhyay, Brij-micelle and polyacrylic acid interaction investigated by Cu^{2+} -induced pyrene fluorescence: Effect of Brij-micelle structure, Chem. Phys. Lett. 476 (2009) 244-248.

[33] A.C. Ferrari, Raman spectroscopy of graphene and graphite: Disorder, electron–phonon coupling, doping and nonadiabatic effects, Solid State Commun. 143 (2007) 47-57.

[34] A.C. Ferrari, D.M. Basko, Raman spectroscopy as a versatile tool for studying the properties of graphene, Nat. Nanotechnol. 8 (2013) 235-246.

[35] L. Stobinski, B. Lesiak, A. Malolepszy, M. Mazurkiewicz, J. Zemek, P. Jiricek, I. Bieloshapka, Graphene oxide and reduced graphene oxide studied by the XRD, TEM and electron spectroscopy methods. J. Electron Spectros. Relat. Phenomena 195 (2014) 145-154.

[36] C. Zhang, D.M. Dabbs, L.-M. Liu, I.A. Aksay, R. Car, A. Sellon, Combined effects of functional groups, lattice defects, and edges in the infrared spectra of graphene oxide. J. Phys. Chem. C 119 (2015) 18167-18176.

[37] F. Tuinstra, J.L. Koenig, Raman spectrum of graphite, J. Chem. Phys. 53 (1970) 1126-1130.

[38] R. Rao, D. Tishler, J. Katoch, M. Ishigami, Multiphonon Raman scattering in graphene, Phys. Rev. B 84(11) (2011) 113406.

[39] R.K. Layek, A.K. Nandi, A review on synthesis and properties of polymer functionalized graphene, Polymer 54 (2013) 5087-5103.

[40] V.N. Popov, 2D Raman band of single-layer and bilayer graphene, 682 (2016) 012013 http://iopscience.iop.org/article/10.1088/1742-6596/682/1/012013/pdf (accessed Apr 12, 2017).

[41] L.M. Malard, M.A. Pimenta, G. Dresselhaus, M.S. Dresselhaus, Raman spectroscopy in graphene, Phys. Rep.-Rev. Sec. Phys. Lett. 473 (2009) 51-87.

[42] A. Mohr, P. Talbiersky, H-G Korth, R. Sustmann, R. Boese, D. Bläser, H. Rehage, A new pyrene-based fluorescent probe for the determination of critical micelle concentrations, J. Phys. Chem. B 111 (2007) 12985-12992.

[43] A.M. Khan, S.S.Shah, Determination of critical micelle concentration (cmc) of sodium dodecyl sulfate (SDS) and the effect of low concentration of pyrene on its cmc using ORIGIN software, J. Chem. Soc. Pak. 30 (2008) 186-191.

[44] J.H. Clint, Surfactant Aggregation. Springer Science & Business Media: New York, 1992; pp 192-221.

[45] A.G. Hsieh, S. Korkut, C. Punckt, I.A. Aksay, Dispersion stability of functionalized graphene in aqueous sodium dodecyl sulfate solutions, Langmuir 29 (2013) 14831-14838.

[46] T. Wu, X. Cai, S. Tan, H. Li, J. Liu, W. Yang, Adsorption characteristics of acrylonitrile, p-toluenesulfonic acid, 1-naphthalenesulfonic acid and methyl blue on graphene in aqueous solutions, Chem. Eng. J. 173 (2011) 144-149.

[47] J. Xu, L. Wang, Y. Zhu, Decontamination of bisphenol A from aqueous solution by graphene adsorption, Langmuir 28 (2012) 8418-8425.

[48] Z. Pei, L. Li, L. Sun, S. Zhang, X. Shao, S. Yang, B. Wen, Adsorption characteristics of 1,2,4-trichlorobenzene, 2,4,6-trichlorophenol, 2-naphthol and naphthalene on graphene and graphene oxide, Carbon 51 (2013) 156-163.

[49] E. Bozkurt, M. Acar, Y. Onganer, K. Meral, Rhodamine 101-graphene oxide composites in aqueous solution: the fluorescence quenching process of rhodamine 101, Phys. Chem. Chem. Phys. 16 (2014) 18276-18281.

[50] J. Wang, Z. Chen, B. Chen, Adsorption of polycyclic aromatic hydrocarbons by graphene and graphene oxide nanosheets, Environ. Sci. Technol. 48 (2014) 4817-4825.

[51] M. de Miguel, M. Álvaro, H. García, Graphene as a quencher of electronic excited states of photochemical probes, Langmuir 28 (2012) 2849-2857.

[52] J.N. Miller, J.C. Miller, Statistics and Chemometrics for Analytical Chemistry. Pearson Education Limited: Harlow, 2010.

[53] J.R. Lakowicz, Principles of Fluorescence Spectroscopy, Springer Science & Bussiness Media: New York, 2006; pp 278-327.

[54] S. Palencia, S. Vera, A. Díez-Pascual, M.P. San Andrés, Quenching of fluorene fluorescence by single-walled carbon nanotube dispersions with surfactants: application for fluorene quantification in wastewater, Anal. Bioanal. Chem. 407 (2015) 4671-4682.

[55] X-F Zhang, F. Li, Interaction of graphene with excited and ground state rhodamine revealed by steady state and time resolved fluorescence, J. Photochem. Photobiol. A 246 (2012) 8-15.

[56] A.M. Díez-Pascual, D. García-García, M.P. San Andrés, S. Vera, Determination of riboflavin based on fluorescence quenching by graphene dispersions in polyethylene glycol, RSC Adv. 6 (2016) 19686-19699.

[57] M.P. San Andrés, A.M. Díez-Pascual, S. Palencia, J. San Torcuato, M. Valiente, S. Vera, Fluorescence quenching of α-tocopherol by graphene dispersed in aqueous surfactant solutions, J. Lumines. 187 (2017) 169-180.

[58] A.M. Díez-Pascual, C. Hermosa, M.P. San Andrés, M. Valiente, S. Vera, Effect of graphene and graphene oxide dispersions in poloxamer-407 on the fluorescence of riboflavin: a comparative study, J. Phys. Chem. C 121 (2017) 830-843.

FIGURES CAPTIONS.

Figure 1. Raman spectra of pristine G (—) and G dispersions in SDS 0.02 mol L^{-1} with w_G/w_S of 0.5% (—), 1% (—) and 2% (—).

Figure 2. SEM micrographs at different magnifications of pristine G (a) and dispersions of G in SDS 0.02 mol L^{-1} with w_G/w_S of 0.5% (b), 1% (c) and 2% (d).

Figure 3. TEM micrographs at different magnifications of G dispersions in SDS 0.02 mol L^{-1} with w_G/w_S of 0.5 % (a), 1 % (b) and 2 % (c).

Figure 4. Normalized fluorescence intensity of pyrene in aqueous SDS solutions at concentrations below and above the CMC.

Figure 5. Normalized fluorescence intensity of pyrene in different dispersions of G in SDS 0.02 mol L^{-1}: a,b) dispersions prepared by dilution in water with w_G/w_S = 0.5 and 2%, respectively. c,d) dispersions prepared by dilution with SDS 0.02 mol L^{-1} with w_G/w_S = 0.5 and 2%, respectively.

Figure 6. a) Normalized fluorescence intensity of pyrene as a function of SDS concentration for the three dispersions of G in SDS 0.02 mol L^{-1} prepared by dilution with water. b) Normalized fluorescence intensity of pyrene vs. G concentration for the three dispersions of G in SDS 0.02 mol L^{-1} prepared by dilution with SDS 0.02 mol L^{-1}. (●aqueous SDS, ▲ 0.5% G, ○ 1% G, ♦ 2% G).

Figure 7. Different steps of surfactant adsorption at the G surface in the presence of pyrene

Figure 8. I/III intensity ratio versus SDS concentration for aqueous surfactant solutions and dispersions of G in SDS 0.02 mol L^{-1}, w_G/w_S constant. The arrow indicates the CMC. (●aqueous SDS, ▲ 0.5% G, ○ 1% G, ♦ 2% G)

Figure 9. F_0/F *vs* G concentration for dispersions of G in SDS 0.02 mol L^{-1} prepared by dilution with SDS 0.02 mol L^{-1}, w_G/w_S variable. Inset: Concentration range of G 0-20 mg L^{-1} (▲G 0.5 %, ○ G 1 %, ♦ G 2 %).

Table I. Parameters of the linear fit to a Stern-Volmer equation type for G dispersions in SDS 0.02 mol L^{-1} at w_G/w_S 0.5, 1 and 2%, [SDS] constant.

w_G/w_S (%)	Intercept ± s	Slope ± s	r	R^2
0.5	0.92±0.02	0.042±0.002	0.992	98.2
1	1.01±0.01	0.038±0.002	0.998	99.5
2	0.92±0.01	0.042±0.002	0.997	99.3

Table IIa. Mean values of slope, standard deviation (s) and relative standard deviation (%RSD) for the three G dispersions, w_G/w_S = 0.5, 1 and 2%, in SDS 0.02 mol L^{-1}.

Dispersion (w_G/w_S)	n	Mean value of slope	s	%RSD
0.5%	6	0.042	0.003	7.86
1%	6	0.042	0.002	4.88
2%	6	0.041	0.002	4.57
Total	18	0.042	0.002	5.70

Table IIb. One-way ANOVA for the three G dispersions, w_G/w_S = 0.5, 1 and 2%, in SDS 0.02 mol L^{-1}.

Source of variation	Sum of squares	Degrees of freedom	Mean square	F	P value
Between-sample	$2.89x10^{-6}$	2	$1.44x10^{-6}$	0.23	**0.798**
Within-sample	$9.47x10^{-5}$	15	$6.31x10^{-6}$		
Total	$9.75x10^{-5}$	17			

FIGURES

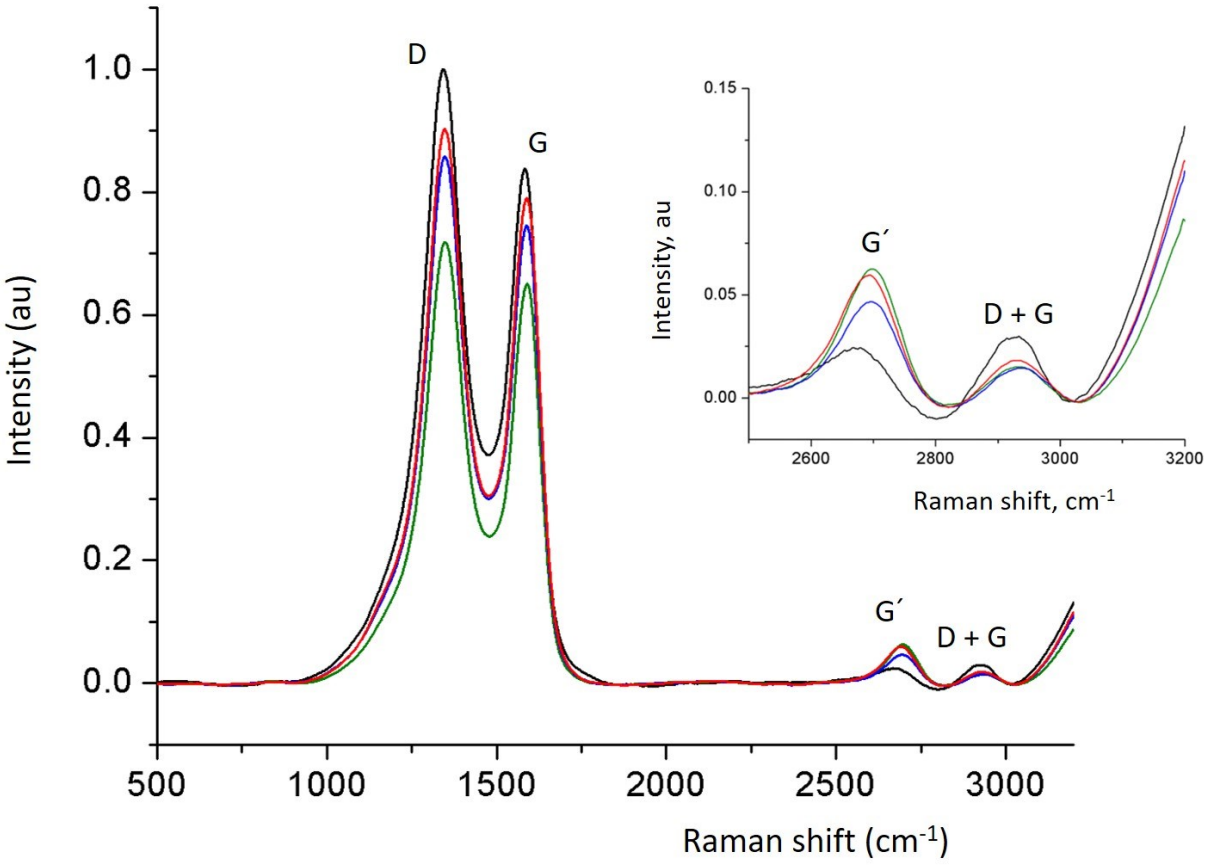

FIGURE 1

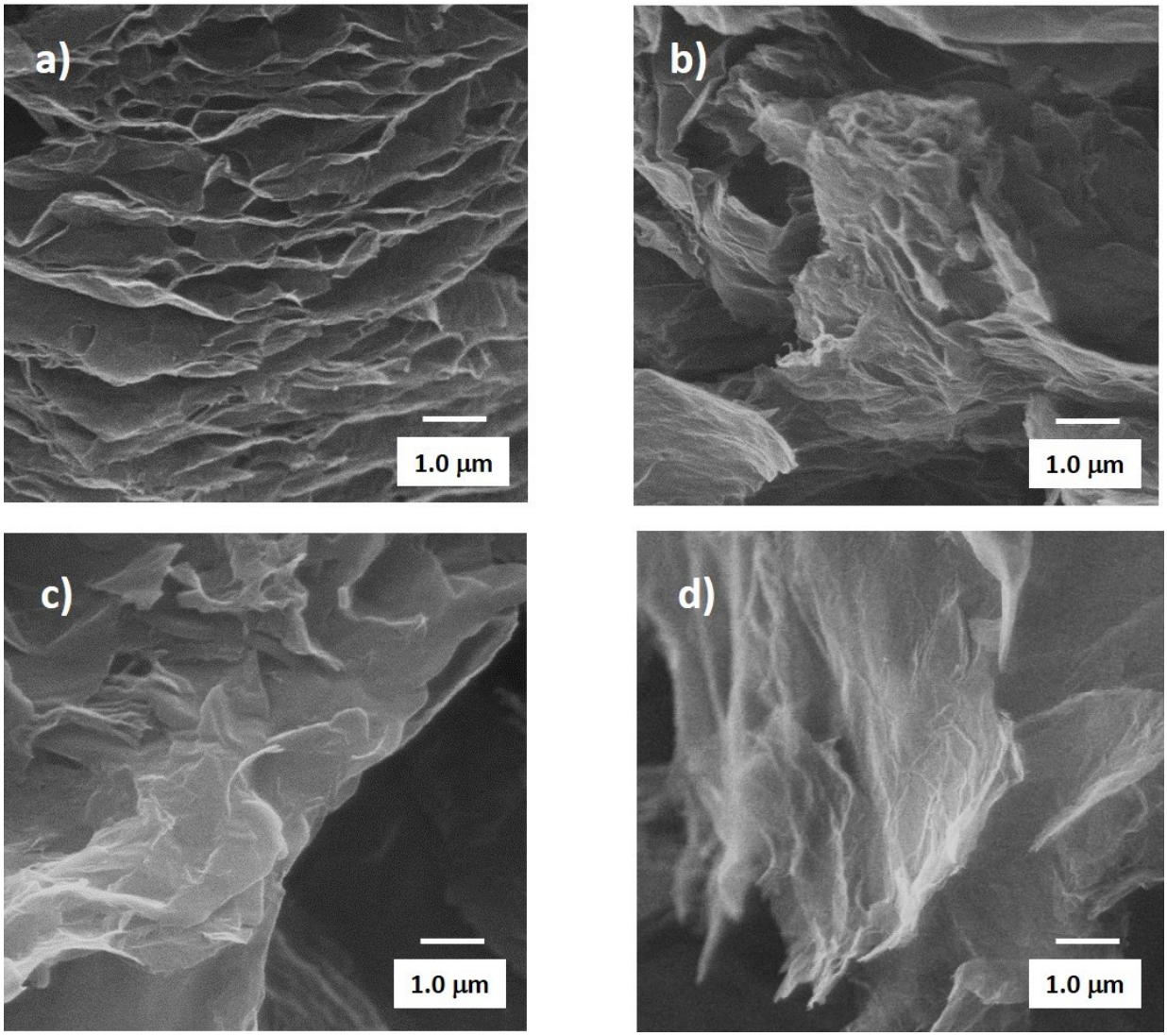

FIGURE 2

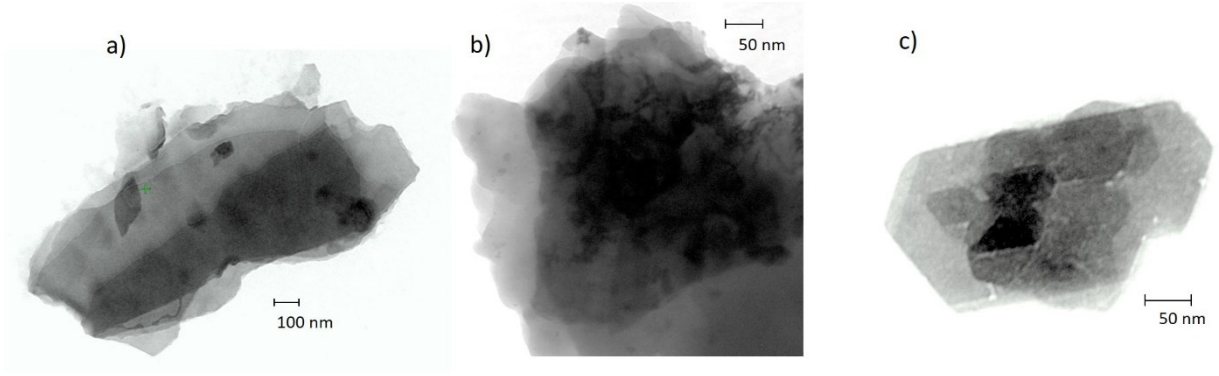

FIGURE 3

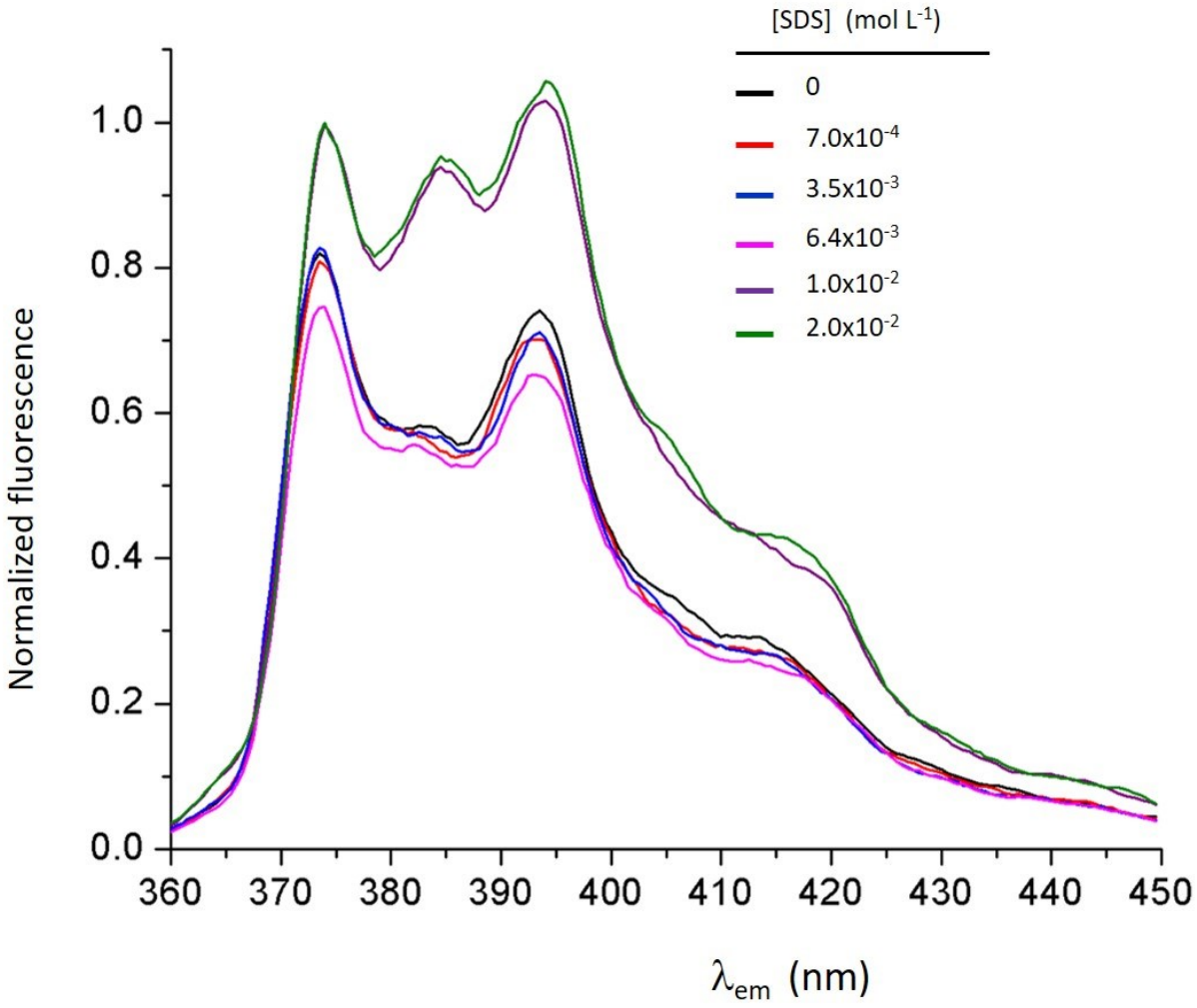
[SDS] (mol L-1)
0
7.0x10-4
3.5x10-3
6.4x10-3
1.0x10-2
2.0x10-2
Normalized fluorescence
1.0
0.8
0.6
0.4
0.2
0.0
360
370
380
390
400
410
420
430
440
450
λem (nm)

FIGURE 4

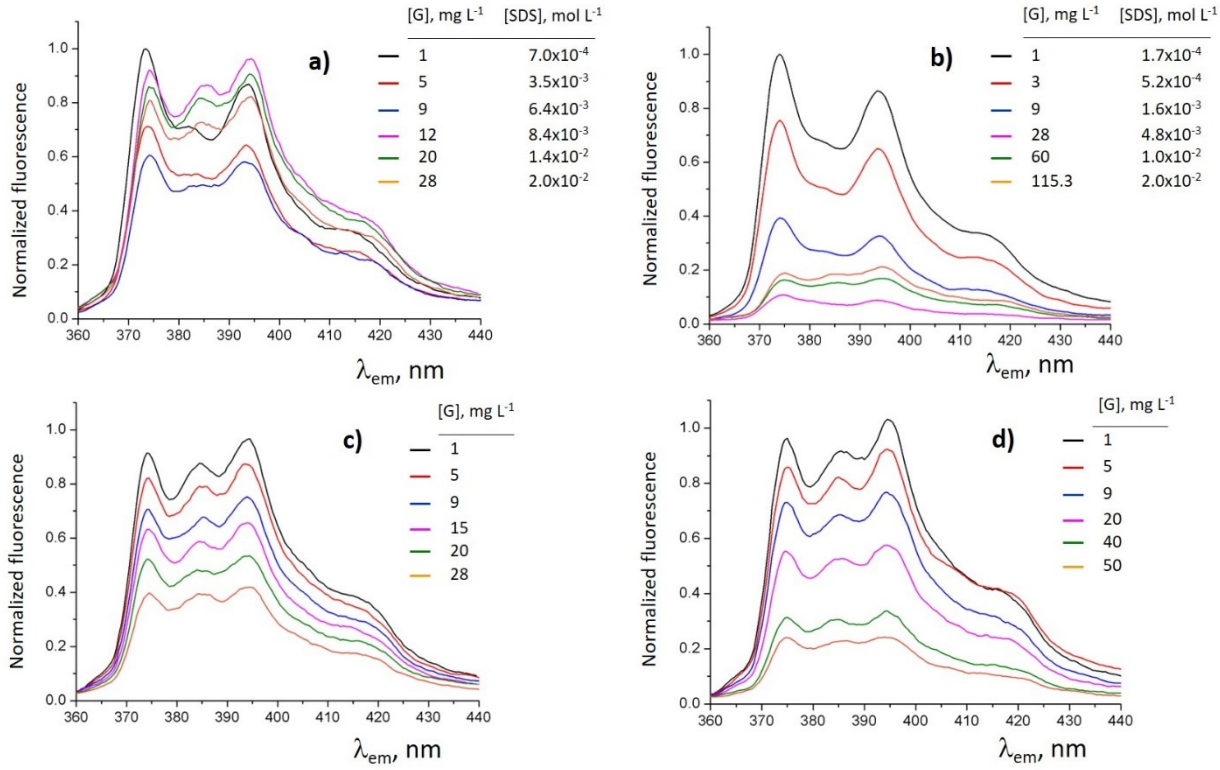
a)
[G], mg L-1
[SDS], mol L-1
1
7.0x10-4
5
3.5x10-3
9
6.4x10-3
12
8.4x10-3
20
1.4x10-2
28
2.0x10-2
b)
[G], mg L-1
[SDS], mol L-1
1
1.7x10-4
3
5.2x10-4
9
1.6x10-3
28
4.8x10-3
60
1.0x10-2
115.3
2.0x10-2
c)
[G], mg L-1
1
5
9
15
20
28
d)
[G], mg L-1
1
5
9
20
40
50
Normalized fluorescence
λem, nm

FIGURE 5

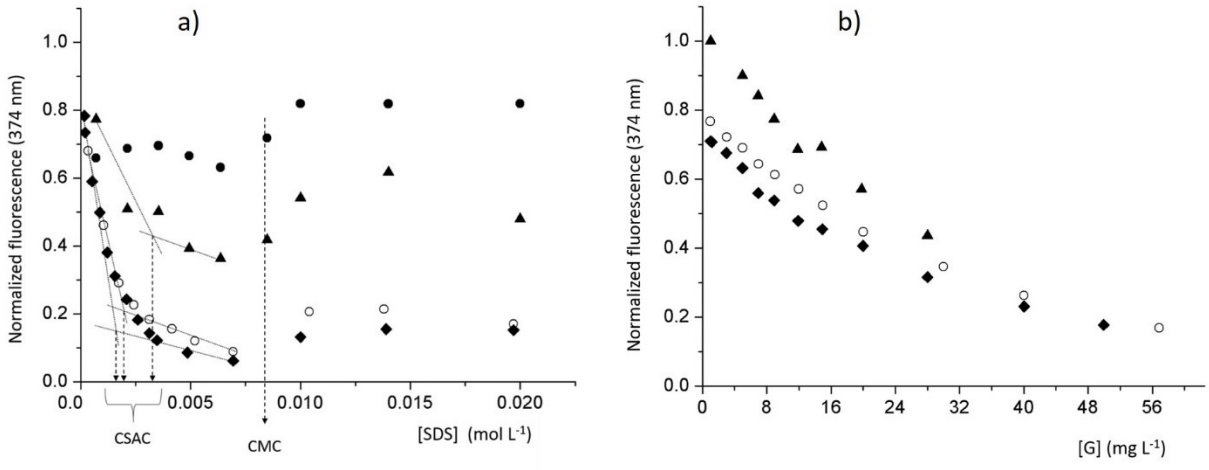
a)
Normalized fluorescence (374 nm)
1.0
0.8
0.6
0.4
0.2
0.0
0.0
0.005
0.010
0.015
0.020
CSAC
CMC
[SDS] (mol L-1)
b)
Normalized fluorescence (374 nm)
1.0
0.8
0.6
0.4
0.2
0.0
0
8
16
24
32
40
48
56
[G] (mg L-1)

FIGURE 6

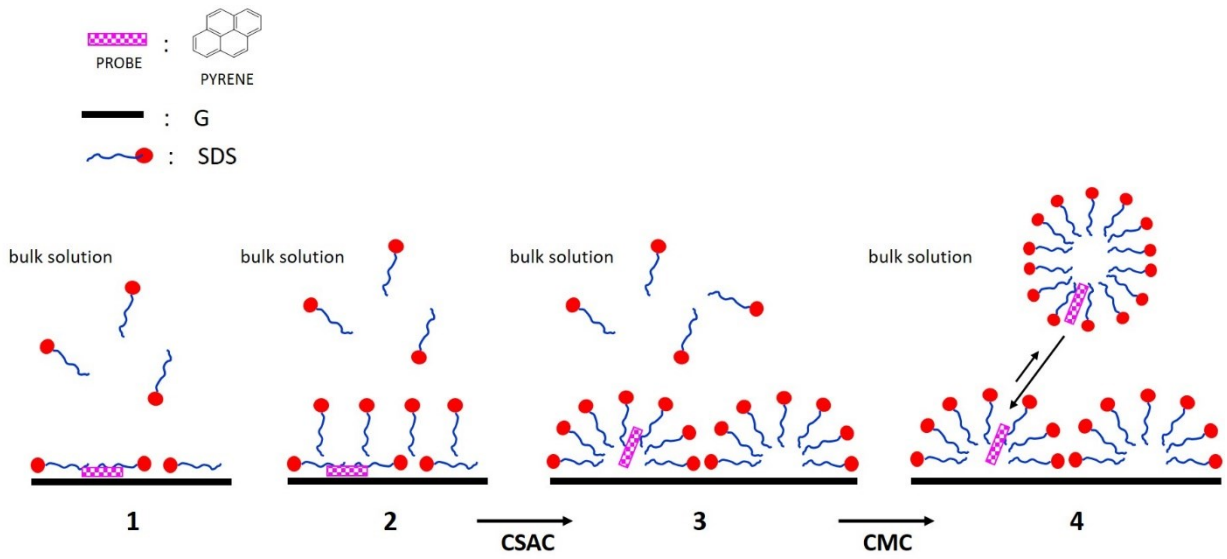
PROBE
PYRENE
G
SDS
bulk solution
bulk solution
bulk solution
bulk solution
1
2
CSAC
3
CMC
4

FIGURE 7

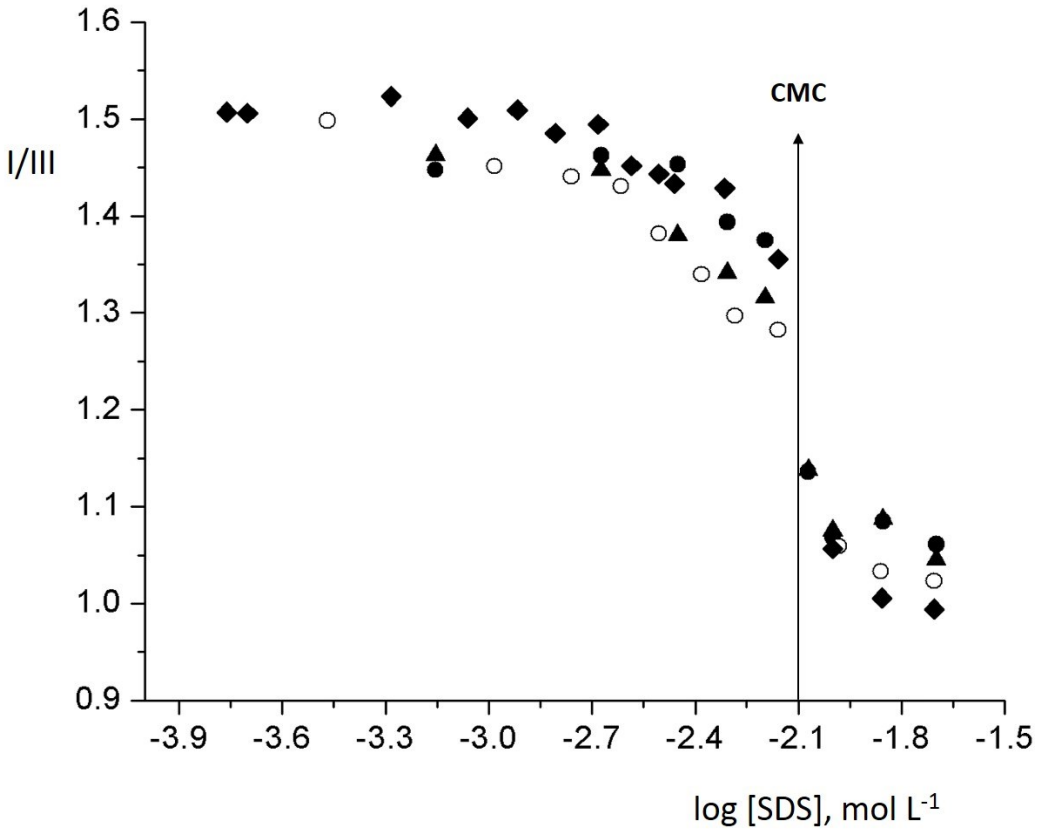
1.6
1.5
1.4
1.3
1.2
1.1
1.0
0.9
I/III
CMC
-3.9
-3.6
-3.3
-3.0
-2.7
-2.4
-2.1
-1.8
-1.5
log [SDS], mol L-1

FIGURE 8

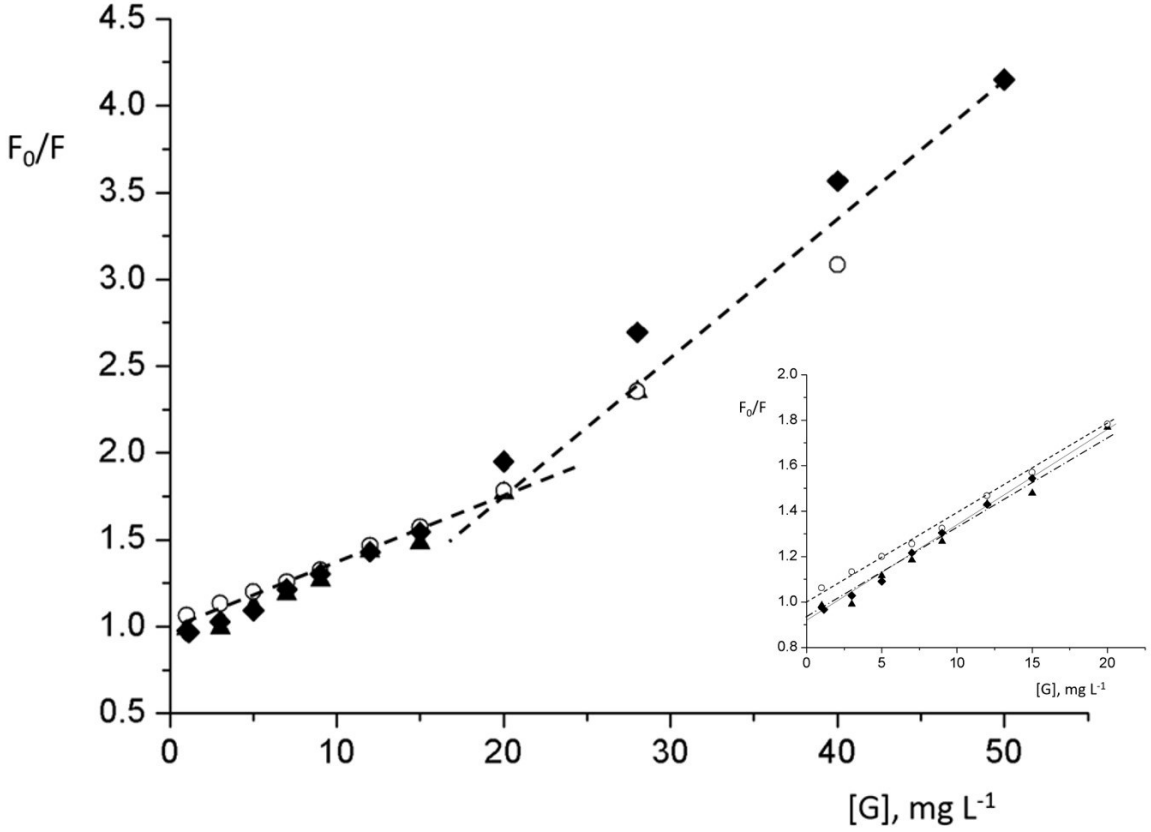
F0/F
4.5
4.0
3.5
3.0
2.5
2.0
1.5
1.0
0.5
0
10
20
30
40
50
[G], mg L-1
F0/F
2.0
1.8
1.6
1.4
1.2
1.0
0.8
0
5
10
15
20
[G], mg L-1

FIGURE 9

SUPPLEMENTARY MATERIAL

STUDY OF GRAPHENE DISPERSIONS IN SODIUM DODECYLSULFATE BY STEADY-STATE FLUORESCENCE OF PYRENE.

S. Vera-López*, P. Martínez, M.P. San Andrés, A. Díez-Pascual, and M. Valiente

Department of Analytical Chemistry, Physical Chemistry, and Chemical Engineering,

University of Alcalá, 28871, Madrid, Spain

*Corresponding author

e-mail: soledad.vera@uah.es

Table S1. Intercept and slope values, with their corresponding standard deviation, correlation coefficient and P value for the two sets of dispersions of G/SDS at w_G/w_S 0.5, 1 and 2%, w_G/w_S constant.

	w_G/w_S 0.5%					
	I (374 nm)		III (385 nm)		V (394 nm)	
Intercept	0.3±0.1		0.18±0.08		0.23±0.09	
Slope	0.7±0.2		0.9±0.1		0.9±0.1	
r	0.856		0.917		0.924	
$P_{value\ for\ Intercept}$	0.010	Reject H_0	0.063	Accept H_0	0.029	Reject H_0
$P_{value\ for\ Slope}$	0.086	Accept H_0	0.699	Accept H_0	0.594	Accept H_0
	w_G/w_S 1%					
	I (374 nm)		III (385 nm)		V (394 nm)	
Intercept	0.02±0.02		0.02±0.01		0.02±0.01	
Slope	0.94±0.04		0.97±0.03		0.95±0.03	
r	0.992		0.993		0.993	
$P_{value\ for\ Intercept}$	0.260	Accept H_0	0.194	Accept H_0	0.292	Accept H_0
$P_{value\ for\ Slope}$	0.153	Accept H_0	0.393	Accept H_0	0.202	Accept H_0
	w_G/w_S 2%					
	I (374 nm)		III (385 nm)		V (394 nm)	
Intercept	-0.07±0.03		-0.05±0.02		-0.07±0.02	
Slope	1.09±0.06		1.10±0.05		1.08±0.05	
r	0.983		0.990		0.986	
$P_{value\ for\ Intercept}$	0.038	Reject H_0	0.017	Reject H_0	0.017	Reject H_0
$P_{value\ for\ Slope}$	0.163	Accept H_0	0.074	Accept H_0	0.156	Accept H_0

Null hypothesis, H_0: Intercept = 0 Alternative hypothesis, H_1: Intercept ≠ 0
Slope = 1 Slope ≠ 1

Table S2. Intercept and slope values, with their corresponding standard deviation, correlation coefficient and P value for the two sets of dispersions of G/SDS at w_G/w_S 0.5, 1 and 2%, fixed [SDS] = 0.02 mol L^{-1} .

	w_G/w_S 0.5%					
	I (374 nm)		III (385 nm)		V (394 nm)	
Intercept	0.05±0.06		0.01±0.09		0.0±0.1	
Slope	0.89±0.09		1.0±0.1		0.9±0.1	
r	0.967		0.939		0.919	
$P_{value\ for\ Intercept}$	0.459	Accept H_0	0.879	Accept H_0	0.703	Accept H_0
$P_{value\ for\ Slope}$	0.277	Accept H_0	0.876	Accept H_0	0.658	Accept H_0
	w_G/w_S 1%					
	I (374 nm)		III (385 nm)		V (394 nm)	
Intercept	0.01±0.01		0.02±0.02		0.02±0.02	
Slope	1.00±0.02		0.98±0.03		0.99±0.03	
r	0.997		0.996		0.996	
$P_{value\ for\ Intercept}$	0.439	Accept H_0	0.227	Accept H_0	0.399	Accept H_0
$P_{value\ for\ Slope}$	0.987	Accept H_0	0.561	Accept H_0	0.684	Accept H_0
	w_G/w_S 2%					
	I (374 nm)		III (385 nm)		V (394 nm)	
Intercept	-0.02±0.04		-0.00±0.03		-0.00±0.04	
Slope	1.02±0.05		0.99±0.04		0.99±0.05	
r	0.988		0.991		0.985	
$P_{value\ for\ Intercept}$	0.613	Accept H_0	0.922	Accept H_0	0.975	Accept H_0
$P_{value\ for\ Slope}$	0.701	Accept H_0	0.939	Accept H_0	0.968	Accept H_0

Null hypothesis, H_0: Intercept = 0 Slope = 1 Alternative hypothesis, H_1: Intercept ≠ 0 Slope ≠ 1

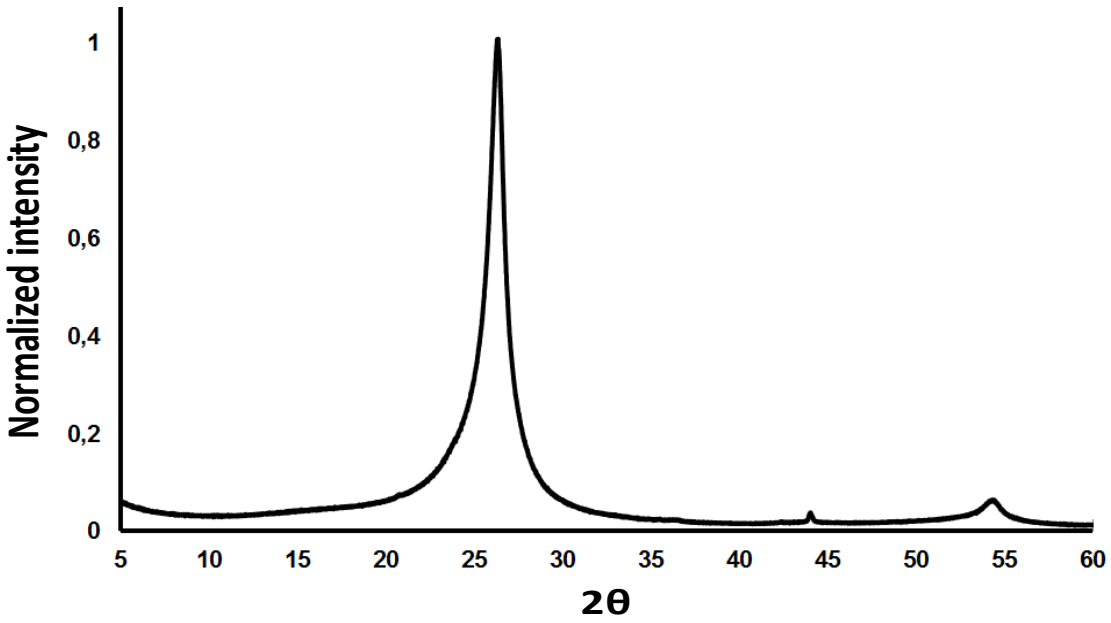

Figure S1. XRD pattern of pristine G provided by Avanzare Innovación Tecnológica

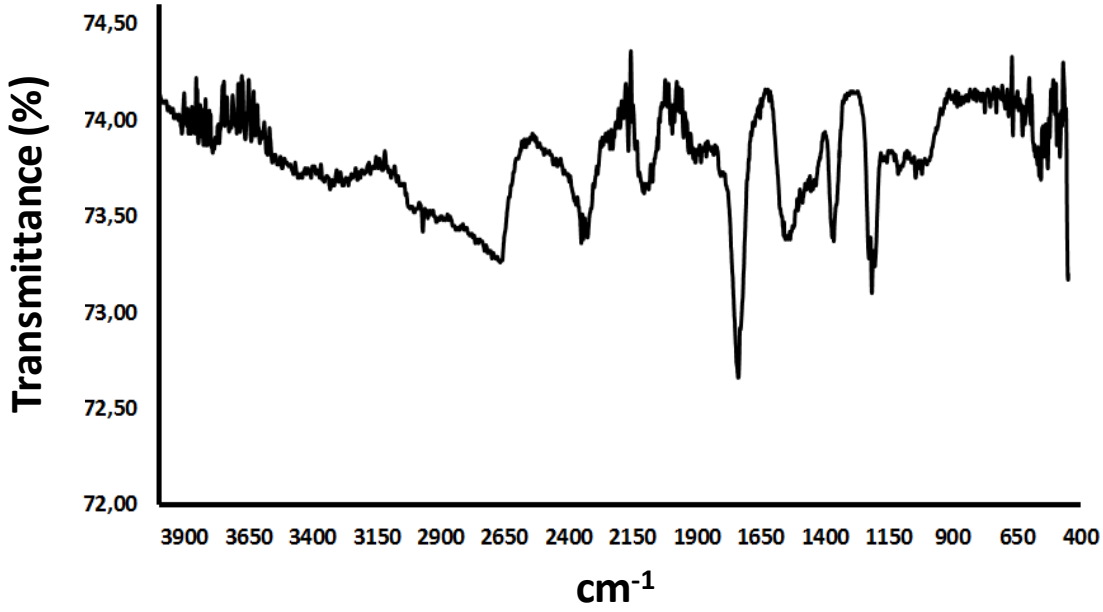

Figure S2. IR spectra of pristine G provided by Avanzare Innovación Tecnológica

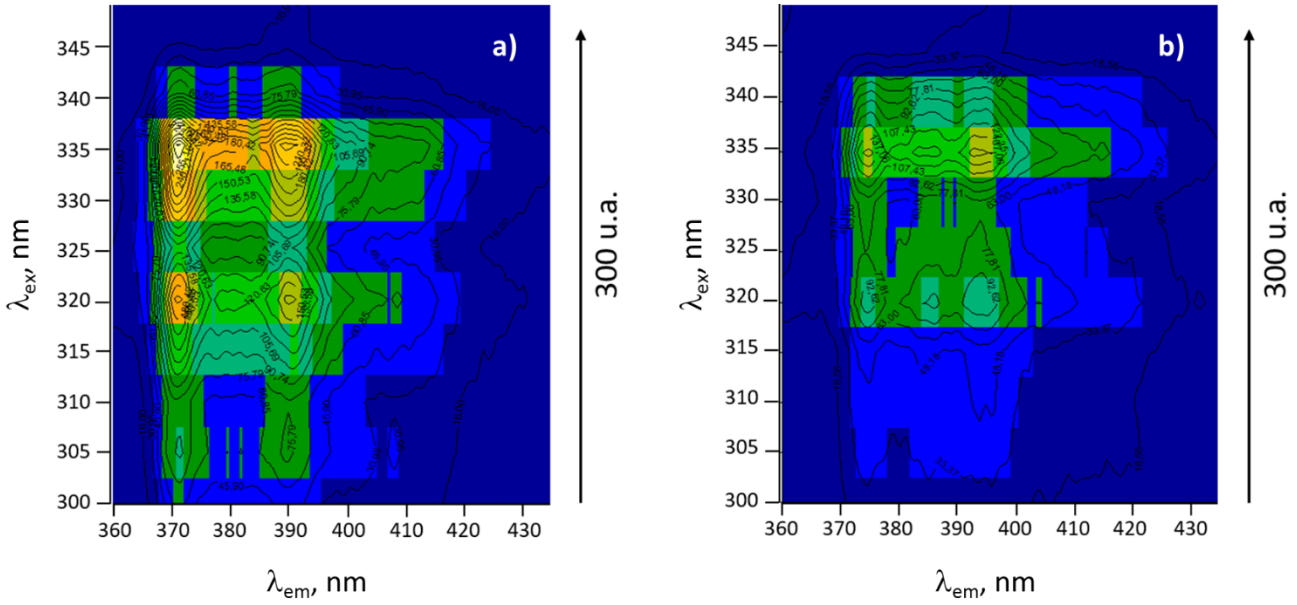

Figure S3. Three-dimensional excitation-emission matrix (3DEEM) fluorescence of pyrene a) in SDS 0.02 mol L^{-1} and b**)** in graphene dispersion, G/SDS (w_G/w_S= 0.5 %).

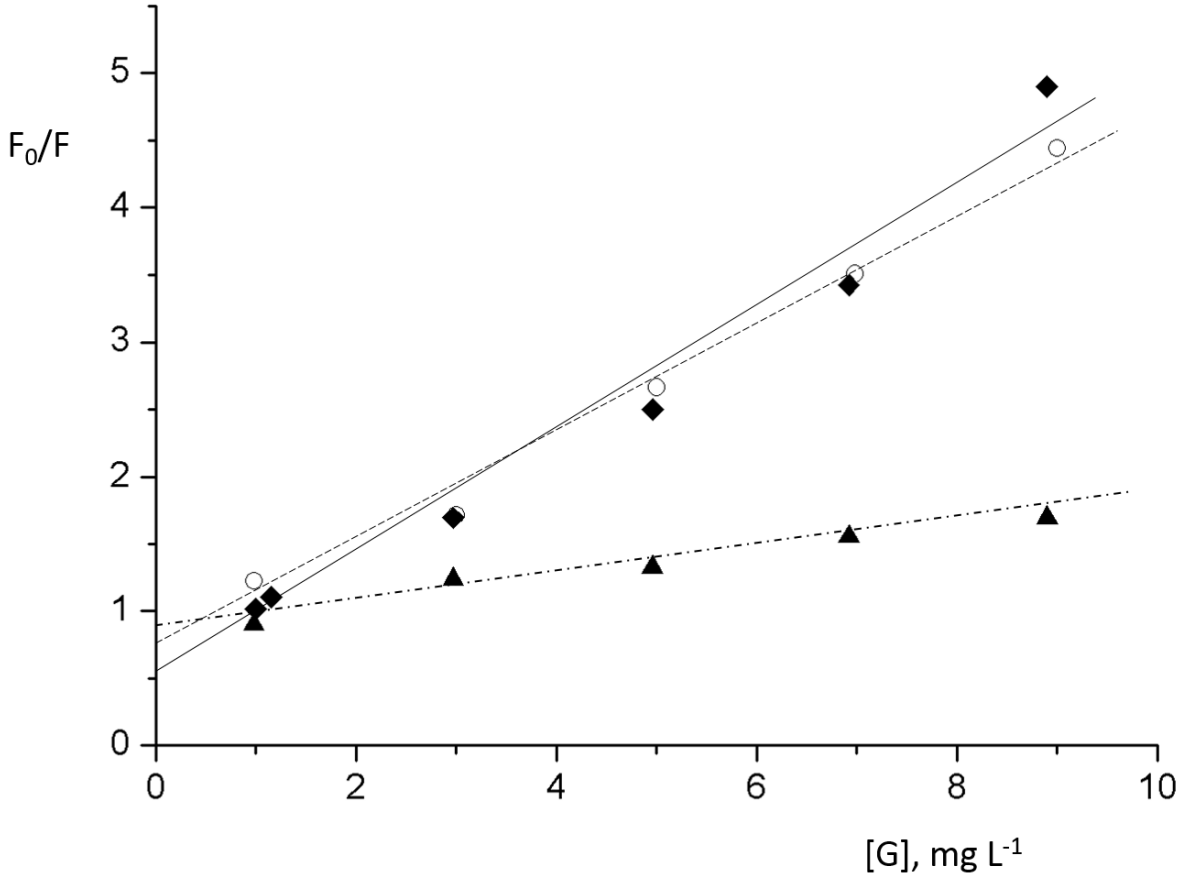

Figure S4. F_0/F *vs* G concentration for dispersions of G in SDS 0.02 mol L^{-1} prepared by dilution with water, w_G/w_S constant. (▲ 0.5% G, ○ 1% G, ♦ 2% G).

ANOVA ANALYSIS

Certain assumptions must be fulfilled to apply an ANOVA test: a) normal distribution of the data and b) the variance of the random error is not affected by the treatment used, known as "the homogeneity of variance". To verify the first assumption, the normal probability was plotted, Fig.S5, and it was confirmed that the data followed a normal distribution. The assumption of homogeneity of variance implies that the variance within each of the populations is equal. To ensure this hypothesis, one of the statistical tests more commonly used is the Levene's test (P=0.05). A P_{value} = 0.424 was obtained, greater than 0.05, which confirms the homogeneity of the variance.

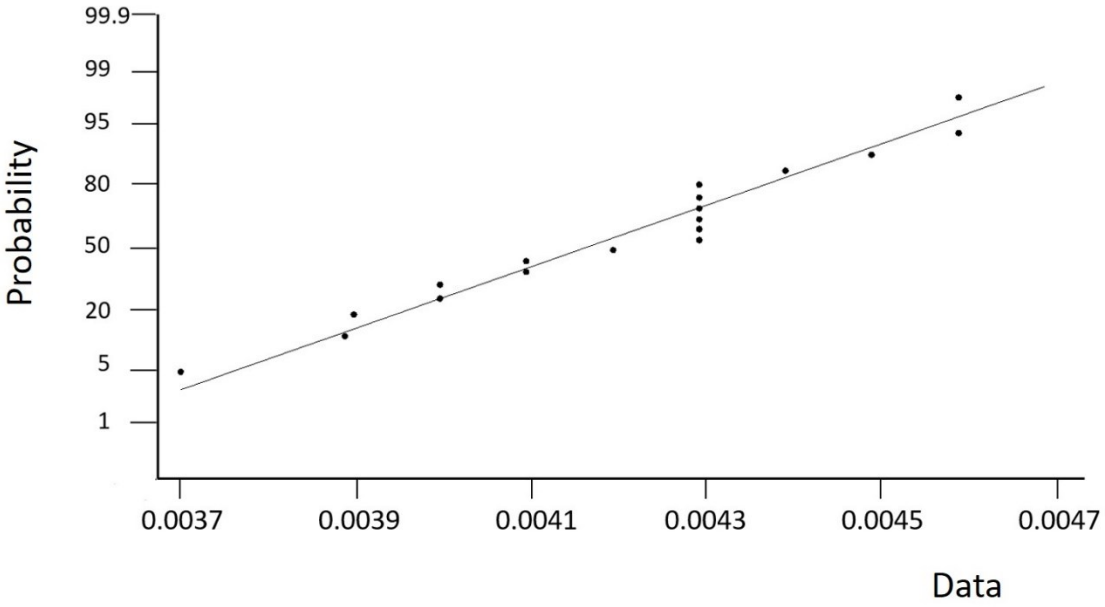

Figure S5. Normality plot